# The Solution Structure of Oxidized Rat Microsomal Cytochrome $b_5$[†,‡]

Fabio Arnesano, Lucia Banci, Ivano Bertini,* and Isabella C. Felli

*Department of Chemistry, University of Florence, Via Gino Capponi 7, 50121, Florence, Italy*

*Received August 1, 1997; Revised Manuscript Received October 17, 1997*[⊗]

ABSTRACT: The solution structure of oxidized rat microsomal cytochrome $b_5$ has been obtained from $^1$H NMR spectra measured at 800 MHz. The available assignment has been extended to 78% of the total protons and 95% of the residues. From 1372 meaningful NOEs, a family of 40 structures has been obtained through the program DYANA; 235 pseudocontact shifts have been then added as further constraints, obtaining an essentially similar family of structures. This latter family has been further refined through restrained energy minimization. The final RMSD values with respect to the average structure are 0.58 ± 0.10 Å and 1.05 ± 0.11 Å for backbone and heavy atoms, respectively. The high quality of the structure allows meaningful comparisons with the solution structure of the reduced protein, with the X-ray and solution structures of the oxidized bovine isoenzyme, and with the solution structure of the apoprotein. Upon loss of one electron, the heme plane undergoes a change in its orientation, possibly due to the change of the total charge. Propionate 7 appears to have a conformation which is dependent on the oxidation state of the iron. Helices α2 and α4 also experience changes in their average positions in the two oxidation states. Finally, the backbone NHs experience different exchange properties in the two oxidation states. While those present in the $\beta$ sheets forming the basis of the heme pocket are nonexchanging in both oxidation states, the NHs in the helices forming the heme-binding pocket are exchanging with the bulk solvent in the oxidized form, indicating larger local mobility in this state. This observation could suggest that, to optimize the electron transfer process, the local mobility should be properly tuned.

The concept of structure for a protein becomes less and less defined the more the structural data are available. Indeed, it is well-known that the detailed structure of a protein in a crystal changes with the symmetry properties of the crystal. The structure of a molecule therefore depends on the interactions with its neighbors. On the other hand, based on the experimental structural constraints, the investigation of the structure of a protein in solution appears quite appealing (*1*−*3*). Indeed, the solution structure can be the basis for studying dynamics in a less rigid frame than the crystal (*4*−*7*). Still, the structure may be sensitive to ionic strength effects, temperature, pH, etc. (*8*, *9*). Recently it was shown that the determination of the solution structure of paramagnetic metalloproteins is possible (*10*, *11*). We have then started looking at the differences between oxidized and reduced forms of electron-transfer proteins (*10*, *12*−*18*), in addition to looking at differences between solid state (when available) and solution. Many differences are noted that eventually may be related to the nature of protein−protein and protein−buffer interactions.

We want to report here the solution structure of the oxidized rat microsomal cytochrome $b_5$ (hereafter cyt $b_5$). Cytochromes are ubiquitous in living organisms (*9*, *19*). Cytochrome $b_5$ is a small hemoprotein bound to the membrane in the endoplasmic reticulum of hepatic cells (*20*). It is found in many mammalian and avian species, and the primary sequence is largely conserved (*21*). The hydrophilic part of cyt $b_5$ contains the heme group (*22*, *23*) and is involved in a wide variety of biological processes. In the endoplasmic reticulum, it participates in the desaturation of fatty acids (*24*, *25*); it supplies electrons to P450 in a number of hydroxylation reactions (*26*, *27*); in erythrocytes, it is found in a soluble form and its function is to reduce methemoglobin (*28*). The hydrosoluble part of the membrane-bound protein can either be obtained through tryptic cleavage (*22*, *23*) or can be expressed in *E. coli* (*20*), and it retains its full activity (*29*). For this reason, it has drawn attention from a large number of researchers, and much data from different approaches are available on it. Therefore, it is an ideal system to address important biological questions. The solution structure of the reduced protein has been determined by our laboratory (*30*). This allows us to compare the solution structure of cyt $b_5$ in the two oxidation states to detect redox state dependent conformational changes. These are related to the reorganization energy which is one of the parameters that determine the electron transfer rate (*31*, *32*). Moreover, besides structural information, NMR also provides dynamic information in solution (*7*, *33*, *34*). This can be achieved from a number of different effects on NMR parameters, the most immediate and easily accessible of

[†] This work was supported by the European Community (Program BIOMED, CT BMH4-CT96-1492), by the HCM Network CHRX-CT94-0540, by the Italian CNR (Biotecnologie e biologia molecolare, CTB CNR 95.02860.CT14), and by MURST.

[‡] The following structural data are available at the Protein Data Bank: 1AW3 (average minimized structure); 1AXX and 2AXX (family of 40 conformers).

* Address correspondence to this author at the Department of Chemistry, University of Florence, Via Gino Capponi 7, 50121, Firenze, Italy. Fax: +39 55 2757555. Telephone: +39 55 2757549. E-mail: bertini@LRM.FI.CNR.IT.

[⊗] Abstract published in *Advance ACS Abstracts,* December 1, 1997.

S0006-2960(97)01896-5 CCC: $15.00 
Published on Web 01/06/1998

which is the NH exchange rate (*35, 36*). The analysis of NH exchange rates in *S. cerevisiae* iso-1 cytochrome *c* revealed a dramatic difference between the two oxidation states, hinting at a different mobility of the protein upon loss/addition of one electron (*37*). It would be interesting to verify whether this is a common behavior for all cytochromes and whether this is related to their biological function, in particular in relation to the mechanism of electron transfer. Electron transfer in biological systems occurs after formation of a complex. Therefore, a structural and dynamic picture of two redox partners in both oxidation states may provide a solid base to understand the factors governing molecular recognition and complex formation in electron transfer proteins.

## MATERIALS AND METHODS

*Sample Isolation and Preparation.* Rat microsomal cytochrome $b_5$ was isolated, using the previously described procedure (*20*), from cultures of *E. coli* strain NM-522 harboring the recombinant pUC13 plasmid containing the gene encoding the 98 amino acid polypeptide corresponding to the soluble part of the microsomal cyt $b_5$ (kindly provided by Dr. S. G. Sligar). About 24 mg of protein, as obtained from the last purification step, was exchanged through ultrafiltration with 1 mM aqueous potassium phosphate buffer, and the pH was gradually adjusted to 7.0. The final concentration was approximately 4 mM. The same procedure was repeated to prepare a sample in $D_2O$.

*NMR Spectroscopy.* $^1$H NMR spectra were acquired on a NMR Bruker Avance800 spectrometer operating at a proton Larmor frequency of 800.13 MHz. To detect connectivities among hyperfine-shifted signals, NOESY experiments (*38, 39*) with a spectral width of 56 ppm in both frequency dimensions, with a recycle time of 470 ms, and with 60 ms of mixing time were acquired. The $^1$H nuclear Overhauser effect (NOE) experiments were performed irradiating at −14.1, at 13.7, and at 11.9 ppm with the superWEFT pulse sequence following the standard procedure (*40*). To optimize detection of connectivities in the diamagnetic region (−3 to 13 ppm), 2D NOESY (*38, 39*) and TOCSY (*41, 42*) spectra were acquired with recycle times of 1.1 s, mixing times of 100 ms, and a spin-lock time of 80 ms, respectively. In the NOESY spectrum acquired on the diamagnetic window, the strong $H_2O$ resonance was suppressed through the WATERGATE sequence (*43*), while in other cases through presaturation. Quadrature detection was achieved by using the TPPI method (*39*). All data consisted of 4K data points in the acquisition dimension and of 198−926 experiments in the indirect dimension. Raw data were weighted with a squared cosine function, zero-filled, and Fourier-transformed to obtain a final matrix of 4096 × 4096 data points. A polynomial base line correction was applied in both dimensions. This set of spectra was collected at 298 K (either on the $H_2O$ or on the $D_2O$ samples) and at 313 K (on the $H_2O$ sample).

Spectra were processed using the standard Bruker software and analyzed on IBM RISC 6000 computers through the XEASY program (*44*).

*Proton−Proton Distance Constraints.* Intensities of dipolar connectivities were mainly measured on the NOESY maps acquired over the diamagnetic window at 298 K in $H_2O$ or in $D_2O$. Dipolar connectivities involving hyperfine-shifted protons were integrated on the NOESY spectrum acquired over the 56 ppm spectral window at 298 K. Intensities of dipolar connectivities were converted into upper distance limits, to be used as input for structure calculations, through the program CALIBA (*45*). Connectivities measured on NOESY maps acquired with different mixing times were calibrated independently. Calibration curves were adjusted iteratively as the calculations proceeded. To dipolar connectivities detected in 1D spectra upon irradiation at −14.1 ppm were assigned upper distance limits of 5 Å . Stereospecific assignments were obtained through the program GLOMSA (*45*) on the preliminary calculated structures.

*Pseudocontact Shift Constraints*. The hyperfine shift, which is the difference between the chemical shift of a nucleus in a paramagnetic compound and the shift that the same nucleus experiences in the analogous diamagnetic one, arises from two mechanisms: contact (*46*) and pseudocontact (*47−50*). The contact contribution is due to the unpaired spin density present on the nucleus itself, and generally it can be neglected a few bonds away from the paramagnetic center (*50*). The pseudocontact contribution arises from the part of the dipolar interaction which is not averaged in solution and depends on the position of a nucleus with respect to the orientation of the magnetic susceptibility tensor (*50*). Within the metal-centered point dipole−point dipole approximation, the following equation holds:

$$\delta_{pc} = \frac{1}{12\pi r_i^3}\left[\Delta\chi_{ax}(3n_i^2 - 1) + \frac{3}{2}\Delta\chi_{rh}(l_i^2 - m_i^2)\right] \quad (1)$$

where $\Delta\chi_{ax}$ and $\Delta\chi_{rh}$ are the axial and the rhombic anisotropies of the magnetic susceptibility induced by the paramagnetic ion, $r_i$ is the distance of the nucleus $i$ from the metal ion, and $l_i$, $m_i$, and $n_i$ are the direction cosines of the position vector of atom $i$ with respect to the orthogonal reference system formed by the principal axes of the magnetic susceptibility tensor. It is possible, in principle, that the metal-centered model is not strictly valid when nuclei are close to the paramagnetic center. In this case, the observed pseudocontact shifts are large. Therefore, we have given a tolerance between the observed and calculated shift, which is proportional to the pseudocontact shift itself (*13*).

Pseudocontact shifts were obtained by subtracting from the chemical shifts of the oxidized form, those of the reduced form available at 313 K (*30*). Hyperfine shifts of the heme, of His 39, and of His 63 were not included in the calculations since they would experience a nonnegligible contact shift.

*Structure Calculations.* The structures were calculated using the modified version of the program DYANA (*51*), suitable for the use of pseudocontact shift restraints, PSEUDYANA (unpublished results from our laboratory). A preliminary family of structures obtained using NOE constraints only was used as an input model to fit eq 1 through the program FANTASIAN (*52, 53*) to the experimentally observed pseudocontact shifts. The fitting was performed separately on each member of the family, and the average values of $\Delta\chi_{ax}$ and $\Delta\chi_{rh}$ were used as starting values in structure calculations. The procedure through which pseudocontact shift restraints were introduced in the calculations is analogous to what was performed for cytochrome *c* (*30*). In particular, no assumption on the position of the metal and therefore on the origin of the tensor is needed. A special

residue, namely LTNS, is defined constituted by a pseudoatom PCN representing the origin of the tensor and three pseudoatoms AX, AY, and AZ placed at a unitary distance from the origin and along three mutually orthogonal directions. These directions define the principal axes of the magnetic susceptibility tensor. This residue was linked to the protein through special linker residues, contained in the standard library, having a null Van der Waals radius to allow penetration in the protein frame, and it was maintained close to the iron atom through an upper-distance limit of 0.2 Å.

To include the heme group in the calculations, a new residue was defined in the amino acid library, and it was bound to the protein through linker residues (as mentioned above for the PCN residue), similarly to the procedure used for the reduced form of the protein (*30*). The two binding histidines are coordinated to the iron atom through upper distance limits of 2.1 Å between the iron and the N$\epsilon$2 of the two His residues. In this way, no angle is imposed between the heme plane and the His−iron bond.

During each simulated annealing step, the program recalculates the position of the metal center together with the orientation of the magnetic axes, the only input data being $\Delta\chi_{ax}$, $\Delta\chi_{rh}$ resulting from FANTASIAN calculations. An upper distance limit of 0.2 Å between the PCN pseudoatom and the iron atom was introduced.

A total of 1810 distance constraints and 235 pseudocontact shift constraints (see later) were used in PSEUDYANA calculations. After each cycle, the magnetic anisotropies were calculated and used as input for other calculations until the final values did not deviate more than 5% from the initial ones. The convergence to a final magnetic susceptibility tensor was reached after a few cycles, depending on the quality of the starting structure for which the first tensor is obtained. The relative weight of the two types of constraints was kept equal; 200 random structures were annealed in 14 000 steps using the above constraints. The 40 structures with the lowest target function constitute the family of structures.

Restrained energy minimization (REM) was then applied to each member of the family using the AMBER Package (*54*). The distance constraints were applied within the molecular mechanics and dynamics module of Sander, and the pseudocontact shifts were included as constraints by means of the module PCSHIFTS (*53*). A force constant of 133.76 kJ mol$^{-1}$ was applied for the distance constraints, and of 418 kJ mol$^{-1}$ was applied for the pseudocontact constraints. The other parameters were set as in previous calculations (*13*, *30*).

The quality of the structure was evaluated in terms of deviations from ideal bond lengths and bond angles and through Ramachandran plots obtained using the programs PROCHECK (*55*) and PROCHECK-NMR (*56*).

Structure calculations and analyses were performed on IBM RISC 6000 computers.

*Computer-Aided Assignment.* In order to speed the assignment procedure of NOESY cross-peaks, once a preliminary structural model was available, this was used to back-calculate, through the program CORMA (*57*), the intensities of dipolar connectivities expected on the basis of the structure, corresponding to the assigned proton resonances. This was used only as a suggestion for possible assignment of cross-peaks between signals already assigned with the standard procedure.

Table 1: Newly Assigned Proton Chemical Shifts (ppm) in the Oxidized Form of Microsomal Rat Cytochrome $b_5$ at 298 K in $H_2O$ at pH 7.0

| residue | HN | Hα | H$\beta$ | others |
|---|---|---|---|---|
| Asp 3 | | | 2.55, 2.45 | |
| Leu 36 | | | 2.46, 2.36 | |
| Glu 38 | | | | H$\gamma$ 2.62, 2.56 |
| His 39 | | | | H$\delta$1 12.64 |
| Pro 40 | | 4.10 | | H$\gamma$ 1.30, −0.44 |
| Gly 41 | | 4.41 | | |
| Leu 46 | | | | H$\gamma$ 2.44 |
| Glu 48 | | | 1.95, 1.85 | H$\gamma$ 2.37, 2.21 |
| Gly 62 | | 5.13, 4.85 | | |
| His 63 | | | | H$\epsilon$ ≈-14.1 |
| Arg 68 | | | | H$\gamma$ 2.57 |
| Leu 70 | | | 1.95, 1.72 | |
| Glu 78 | | | | H$\gamma$ 2.08 |
| Leu 79 | | | | H$\gamma$ 1.61; $\delta$CH$_3$ 0.89, 0.60 |
| Pro 81 | | 3.65 | 2.10, 1.66 | H$\gamma$ 1.32, 1.47; H$\delta$ 2.20 |
| Asp 82 | | 2.62, 2.56 | | |
| Lys 89 | | 4.58 | 1.80 | H$\gamma$ 1.69, 1.67 |
| Ser 91 | 8.44 | 4.41 | 3.84 | |

## RESULTS

*Sequence-Specific Assignment.* Extensive assignments of oxidized cyt $b_5$ are available in the literature both for the diamagnetic part of the protein (*58*−*61*) and for hyperfine-shifted signals (*62*−*64*). This study was performed on a 1 mM phosphate buffer, pH = 7.0, sample. In these conditions, besides the two known forms in which cyt $b_5$ exists in solution due to two conformations of the heme ring differing by a 180° rotation around the α−$\gamma$ axis (*65*, *66*), two more minor species (about 20% of the major species) were identified, which are very similar to forms A and B, respectively. These species differ in chemical shift from the major species by not more than 0.5 ppm and are localized mainly around the heme and in a few specific regions of the protein. The study of these minor species is not the aim of this work, and it did not prevent assignment of the major forms A and B. About 90% of the proton resonances of these two major forms are very similar to those reported in the literature and could be easily located in the maps. For a larger number of residues than for those already reported in the literature (56% instead of 45%), the two forms could be resolved, since all spectra were acquired with a higher resolution at 800 MHz. We will focus hereafter on form A which has roughly a 60% population. A few amino acids have a slightly different chemical shift and were found by the standard comparison of NOESY and TOCSY experiments. The assignment was extended with respect to data in the literature to more resonances or whole residues in the proximity of the heme (39, 40, 41, 62, 63) and to some residues in the terminal part of the protein (81, 89, 91). This is reported in detail in Table 1. Ser 18 was not identified, consistent also with what was recently reported (*61*). The total number of assigned residues is 89, which resulted in 78% of the total protons. All the observed NOE cross-peaks above a given treshold have been assigned, besides those falling under the water resonance or those too close to the diagonal. Furthermore, all the NOEs expected above a given threshold on the basis of the calculated structures (see later) have been assigned (with the same exceptions as above).

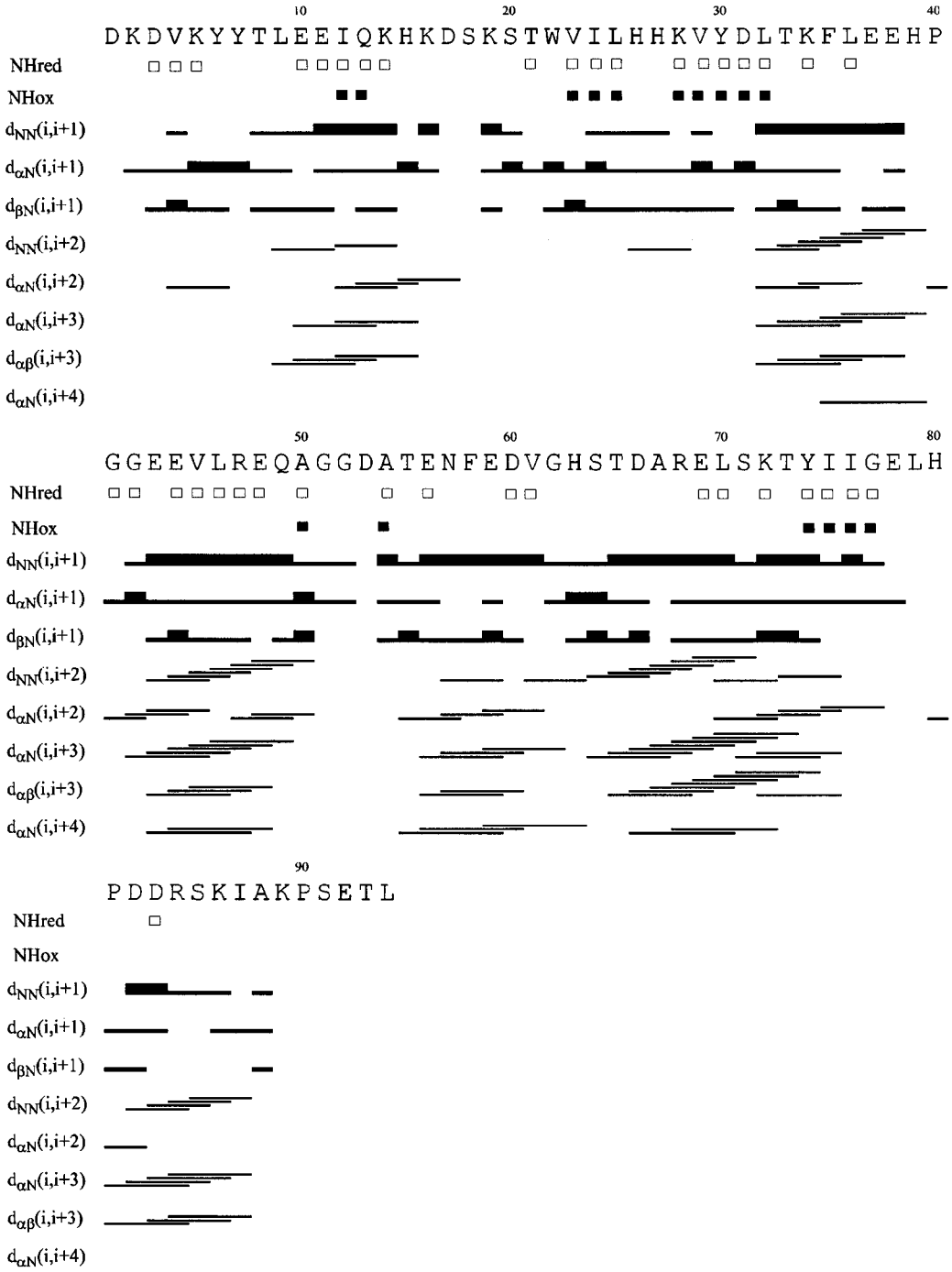


FIGURE 1: Schematic representation of the sequential and medium-range NOE connectivities involving NH, Hα, and H$\beta$ protons. The thickness of the bar indicates the intensity of NOEs. The filled squares represent the nonexchangeable NH protons in the oxidized form, while the open squares are the nonexchangeable NHs of the reduced form (unpublished results of this lab).

*Secondary Structure.* The elements of secondary structure can already be identified by analyzing the pattern of assigned NOEs (*1*). Short- and medium-range NOEs were used to generate Figure 1. In general, $\beta$ strands are expected to give strong $d_{\alpha N}$ sequential and intraresidue connectivities and weak $d_{NN}$ connectivities, while helical structures can be identified by the high number of sequential and medium-range connectivities such as $d_{NN}(i,i+1)$, $d_{NN}(i,i+2)$, $d_{\alpha N}(i,i+3)$, $d_{\alpha N}(i,i+4)$, and $d_{\alpha\beta}(i,i+3)$. Six elements of helical secondary structure can be predicted similarly to the characteristic secondary structural elements present in all the cyt $b_5$ crystal and solution structures (*30, 67*−*71*). These are commonly referred to as helices α1...α6, and, in this particular case, they involve residues 9−15, 32−39, 43−49, 55−63, 64−75, and 81−87. Although there are some discrepancies with previously reported NOE connectivities (*61*), possibly due to different experimental conditions, the results are essentially similar, besides the length of a few helices. The pattern of long-range NOEs (data not shown) points out the existence of a $\beta$ pleated region centered around two antiparallel $\beta$ strands (21−25 and 28−32), the former also being parallel to segment 51−54, the latter antiparallel to region 75−79. Finally, connectivities indicating an antiparallel $\beta$ strand are observed for residues 78−80 and 6−8. Nonexchanging amide protons (that could still be observed in the $D_2O$ sample 5 days after it was prepared)

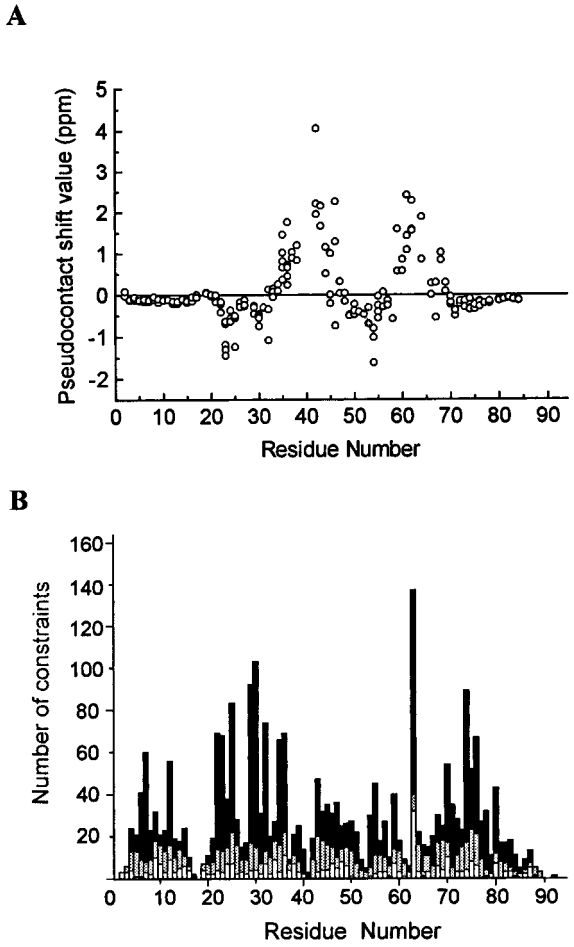


FIGURE 2: (A) Experimental values of pseudocontact shift constraints per residue used in structural calculations. (B) Number of meaningful NOE-derived constraints used in the structural calculations. White, gray, dark gray, and black vertical bars represent respectively intraresidue, sequential, medium-range, and long-range connectivities. Histidine 63 includes connectivities involving the heme.

were found for all the residues in stretches 23−25, 28−32, and 74−77, in agreement with tight elements of $\beta$ secondary structure, and at positions12−13, 50, and 54.

*Solution Structure Calculations.* A total of 3294 NOESY cross-peaks were integrated and transformed into upper distance limits through the program CALIBA (*45*). In the final calibration, volumes were found to be proportional to $1/r^{\wedge 6}$ except for those involving side chain intraresidue connectivities which were proportional to $1/r^{\wedge 5}$. Of the 1810 distance limits, 1372 (an average of 15.5 per assigned residue) were found to be relevant and used in the structure calculations together with 235 pseudocontact shifts. The number of NOEs and the pseudocontact shifts per residue are shown in Figure 2. A total of 27 stereospecific assignments were obtained through the program GLOMSA (*45*) during the course of the calculations, and 10 iterations of PSEUDYANA were performed before the magnetic anisotropy tensor reached convergence. The resulting family of 40 structures has RMSD values to the mean structure (hereafter, unless specified, RMSD values will always be referred to the mean structure) of 0.59 ± 0.10 Å and 1.05 ± 0.11 Å for backbone and heavy atoms, respectively (calculated for residues 4−84). The target function lies in the range 0.19−0.49 Å$^2$ (average target function of 0.37 ± 0.09 Å$^2$).

Table 2: Parameters Characterizing the Solution Structure of Oxidized Microsomal Rat Cyt $b_5$ Obtained in This Work

| | |
|---|---|
| backbone RMSD[a] (Å) | 0.58 ± 0.10 |
| all heavy atoms RMSD[a] (Å) | 1.05 ± 0.11 |
| average target function[b] (Å$^2$) | 0.28 ± 0.14 |
| largest residual NOE violation (Å) | 0.29 |
| largest residual psudocontact shift violation (ppm) | 0.33 |
| residues in most favored Ramachandran plot regions (%) | 77.1 |
| residues in allowed Ramachandran plot regions (%) | 18.6 |
| residues in generously allowed Ramachandran plot regions (%) | 1.4 |
| residues in disallowed Ramachandran plot regions (%) | 2.9 |

[a] RMSD values are calculated for residues 4−84. [b] Corresponding to a REM penalty function of 35.73 ± 4.50 kJ/mol. [c] Ramachandran plot parameters have been obtained on the REM family of structures with the program PROCHECK NMR (Laskowski et al. ,1996), and Gly and Pro are excluded from the Ramachandran analysis.

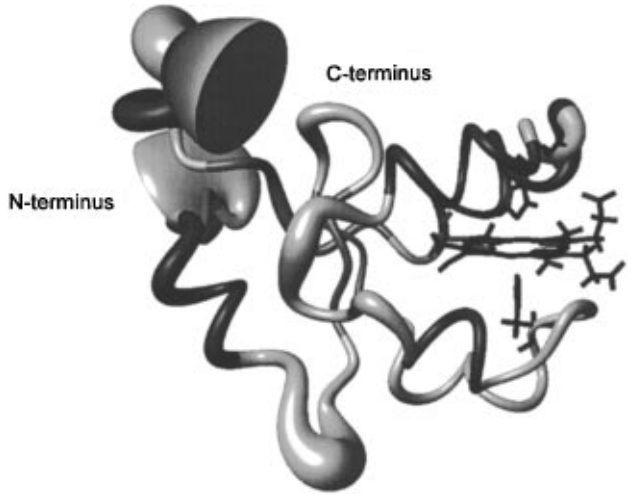


FIGURE 3: REM family of structures of rat cyt $b_5$ (A form). The figure was generated with the program MOLMOL (*90*), and the radius of the tube is proportional to the RMSD.

The contribution of pseudocontact shift constraints with respect to that of NOE constraints to the target function was smaller than 5%.

Restrained energy minimization (REM) yields a family with an average penalty function of 35.73 ± 4.50 kJ mol$^{-1}$ (22.61−63.00 kJ mol$^{-1}$), corresponding to a target function of 0.28 ± 0.14 Å$^2$ (0.17−0.47 Å$^2$), the contribution of pseudocontact shifts being lower than 15% compared to that of NOE constraints. The average RMSD decreases slightly for backbone atoms (0.58 ± 0.10 Å ) and remains the same for heavy atoms. The improvement is mainly localized in the regions of the protein where pseudocontact shift constraints were used, in particular in region 55−74. The parameters describing the quality of the structure are summarized in Table 2. A calculation with only NOE-derived constraints yields a family with a comparable target function (0.15−0.39 Å$^2$) and higher RMSD (0.61 ± 0.12 and 1.06 ± 0.12 Å for backbone and heavy atoms, respectively). The two structures are very similar, with the RMSD between the two average structures being 0.29 Å for backbone atoms (see later).

The solution structure is characterized by high resolution, even in regions close to the paramagnetic center (Figure 3). The RMSD values per residue for the backbone and heavy atoms are reported in Figure 4A. Ser 18 was not identified

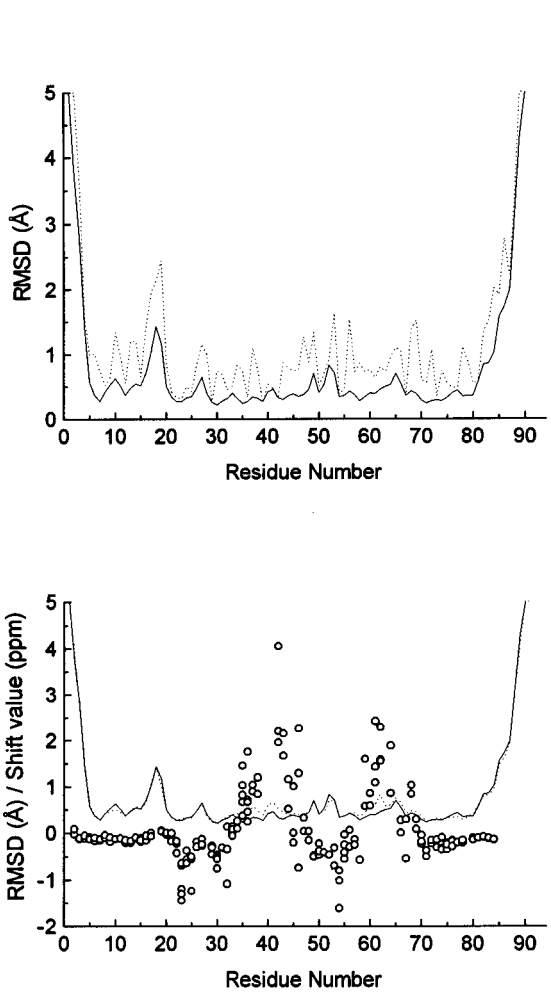


FIGURE 4: (A) RMSD values per residue to the mean structure, for the REM family of structures for backbone (solid line) and for all heavy atoms (dashed line). (B) Backbone RMSD values per residue, to the mean structure, for the REM family (solid line) are compared with those calculated for the family obtained without using pseudocontact shift constraints (dotted line). Also the values of pseudocontact shifts are reported in the figure as circles.

in the oxidized state, and therefore it is not characterized by high resolution. It lies in the edge of an external loop at more than 7 Å from the metal ion. Therefore, it could have escaped detection not because of paramagnetic effects, but probably due to local mobility. The overall folding of the protein is that typical of cyt $b_5$ proteins. Assignment of secondary structure elements was achieved through the PROCHECK analysis which relies on the method of Kabsh and Sander (*72*). The two axial histidines (His 39 and His 63), which are coordinated to the heme, are located between two helices. His 39 follows a series of turns, starting at position 33 that, for simplicity, will be indicated as helix α2 (33−39), even if they cannot be classified as a canonical α helix, as already noted for crystal structures of cyt $b_5$ from different sources (*67*, *70*), and is followed by helix α3 (42−50). His 63 separates helix α4 (54−62) from helix α5 (64−74). Of the elements of $\beta$ secondary structure suggested by the pattern of long-range NOEs, only four segments of extended chain forming a $\beta$ pleated region are observed for residues 5−7, 75−78, 21−25, and 28−32 and are commonly referred to as strands $\beta$1...$\beta$4. Strands $\beta$1 and $\beta$2 are parallel, while strands $\beta$3 and $\beta$4 are antiparallel, connected by a type I turn. This $\beta$ sheet, together with the above mentioned four helices, forms the heme binding pocket. Two more peripheral helices are found for residues 8−14 and 81−87.

It is interesting to compare the average structure of this family with that obtained excluding pseudocontact shift restraints from the calculations. Figure 4B reports the RMSD per residue within each of the two families together with the pseudocontact shifts used. Improvement in the resolution of the solution structure can be observed for most of the residues for which a pseudocontact shift constraint was used. Improvement becomes more evident in the regions around the two heme-binding histidines, where the pseudocontact shifts are larger in absolute value, indicating proximity to the heme itself. The RMSD values between the average structures of the two families are 0.29 and 0.35 Å for backbone and heavy atoms, respectively. This lies within the precision achieved for each family, indicating that, besides an increase in the resolution upon addition of pseudocontact shift constraints, the two structures are virtually identical.

*Comments about the Magnetic Susceptibility Tensor*. The final $\Delta\chi_{ax}$ and $\Delta\chi_{rh}$ values are $(2.83 \pm 0.02) \times 10^{-32}$ m$^3$ and $(-1.06 \pm 0.01) \times 10^{-32}$ m$^3$, respectively. The *z* axis of the magnetic susceptibility tensor is nearly aligned to the perpendicular to the mean heme plane, making with it an angle of 2.5°, while the *x* axis makes an angle of 12.7° with the α−$\gamma$ meso direction. The $\Delta\chi_{ax}$ and $\Delta\chi_{rh}$ values are slightly lower than the ones previously reported in the literature for rat microsomal cyt $b_5$ [$\Delta\chi_{ax} = 3.11 \times 10^{-32}$ m$^3$, $\Delta\chi_{rh} = -1.61 \times 10^{-32}$ m$^3$ (*59*); $\Delta\chi_{ax} = 3.04 \times 10^{-32}$ m$^3$, $\Delta\chi_{rh} = -1.36 \times 10^{-32}$ m$^3$ (*64*)] which were obtained by fitting the pseudocontact shifts observed for the A form of rat microsomal cyt $b_5$ to the crystal structure of the bovine isoenzyme that, as mentioned above, has a 94% homology with the rat isoenzyme. The *y* axis was found to form an angle of −60.7° in the iron−N$\gamma$ direction, which compares very well to the angle of −57.7° found in our fitting. They also result in satisfactory agreement with those found from analysis of the $^{13}$C contact shifts of the heme methyls through MO calculations based on $D_{4h}$ symmetry with a rhombic perturbation (*64*). In that approach, the *z* axis was assumed to be perpendicular to the heme plane, which seems to be a good approximation in the light of the current results (2.5°). The magnetic *y* axis (in the heme plane) is then rotated in the opposite direction, with respect to the iron−N$\gamma$ direction, relative to the rhombic perturbation and is roughly aligned to the bisector to the normals of the histidine rings (*73*). In our solution structure, the angle between the average normal to the two histidine planes and the iron−N$\gamma$ direction is 56.1°. In the crystal structure of the oxidized bovine protein, the same angle is 53.5°. On the other hand, the $\chi_y$ direction, in the present fitting, makes an angle of −57.7° with the iron−N$\gamma$ direction, which indicates that the histidine plane orientation is completely consistent with the above analysis.

Having the magnetic susceptibility tensor available, the pseudocontact contribution to the hyperfine shift can be calculated also for protons belonging to the heme moiety and to the binding histidines. This allows us to evaluate the sum of the contact plus the ligand-centered pseudocontact contributions to the hyperfine shift (Table 3). Looking at the $CH_3$ contact shifts, it is evident that the largest unpaired spin density is located on the $3CH_3$ and $5CH_3$. In the case of *c*-type cytochromes, the $CH_3$ groups with the largest spin

Table 3: Separation of the Contact[a] and Pseudocontact Contributions to the Hyperfine Shift[b]

| atom name | residue name | chemical shift, oxidized species (ppm) | chemical shift, reduced species (ppm) | hyperfine shift (ppm) | calculated pseudocontact shift (ppm) | contact[a] shift (ppm) |
|---|---|---|---|---|---|---|
| HN | His 39 | 9.02 | 5.99 | 3.02 | 2.39 | 0.63 |
| Hα | His 39 | 6.81 | 2.44 | 4.37 | 3.82 | 0.55 |
| Hβ1 | His 39 | 16.5 | 0.80 | 15.70 | 5.89 | 9.81 |
| Hβ2 | His 39 | 7.56 | 0.39 | 7.17 | 5.85 | 1.32 |
| Hδ1 | His 39 | – | – | – | 10.90 | – |
| Hε1 | His 39 | – | – | – | 23.48 | – |
| Hδ2 | His 39 | – | – | – | 18.50 | – |
| HN | His 63 | 11.11 | 5.98 | 5.13 | 2.94 | 2.19 |
| Hα | His 63 | 7.51 | 2.57 | 4.94 | 4.18 | 0.76 |
| Hβ1 | His 63 | 10.53 | – | – | 6.21 | – |
| Hβ2 | His 63 | 9.94 | – | – | 6.69 | – |
| Hδ1 | His 63 | 12.64 | – | – | 9.60 | – |
| Hε1 | His 63 | −12.92 | 0.76 | −13.68 | 13.26 | −26.94 |
| Hδ2 | His 63 | – | – | – | 19.32 | – |
| 8-CH3 | heme | 2.84 | 3.65 | −0.81 | −2.82 | 2.01 |
| 1-CH3 | heme | 10.33 | 3.27 | 7.06 | −1.54 | 8.60 |
| 2-HCα | heme | 26.18 | 7.38 | 18.8 | −4.47 | 23.27 |
| 2−HCβ(trans) | heme | −6.32 | 5.40 | −11.72 | −1.71 | −10.01 |
| 2-HCβ(cis) | heme | −6.66 | 5.05 | −11.71 | −1.72 | −9.99 |
| α-meso | heme | −3.17 | 9.27 | −12.44 | −11.84 | −0.60 |
| 3-CH3 | heme | 14.66 | 3.36 | 11.30 | −4.67 | 15.97 |
| 4-HCα | heme | 4.31 | 8.26 | −3.95 | −2.66 | −1.29 |
| 4−HCβ(trans) | heme | 2.84 | 6.03 | −3.19 | −1.58 | −1.61 |
| 4-HCβ(cis) | heme | 2.60 | 5.94 | −3.24 | −2.66 | −0.58 |
| β-meso | heme | 9.32 | 9.77 | −0.54 | −3.82 | 3.28 |
| 5-CH3 | heme | 19.66 | 3.49 | 16.17 | −1.50 | 17.67 |
| γ-meso | heme | −0.69 | 9.30 | −9.99 | −12.30 | 2.31 |
| 7-Hα | heme | 19.30 | 4.29 | 15.10[c] | −5.88 | 20.98 |
| 7-Hα′ | heme | −1.23 | 4.11 | −5.43[c] | −4.01 | −1.42 |
| 6-Hα | heme | 15.49 | 4.00 | 11.58[c] | −4.72 | 16.30 |
| 6-Hα′ | heme | 14.19 | 3.82 | 10.28[c] | −2.79 | 13.07 |

[a] This term includes ligand-centered pseudocontact shifts. [b] The data are reported for cytochrome $b_5$ at 313 K. Except for the two histidines, for which all calculated pseudocontact shifts are reported, the data are not shown in cases where a proton was not assigned either in the reduced or in the oxidized species. [c] Since stereospecific assignment for propionate diastereotopic pairs is not available for all protons, the average shift of each methylene pair in the reduced form was taken as the diamagnetic reference.

density are 8 and 3 (*13*). This change in the pattern clearly reflects the change in the orientation of the axial ligands, whose projections are roughly rotated by 90°. The Hε1 of His 63 experiences a large positive pseudocontact shift. As has already been pointed out (*13*, *74*), the pseudocontact shifts of the ortho-like histidine protons strongly depend on the tilt of the $\chi_z$ axis with respect to the heme normal. Indeed, in this case, as the tilt angle is very small, the shift is calculated larger than in the case of horse heart cytochrome *c* and much larger than the *S. cerevisiae* cytochrome *c* where the tilt was significant. The similar values of calculated pseudocontact shifts indicate that the histidine ring pseudocontact shifts are essentially not affected by the orientation of the histidine ring planes and consequently by the rhombic anisotropy.

## DISCUSSION

*Comparison with the Reduced Form.* The solution structure of rat microsomal cyt $b_5$ in the reduced state has been recently solved by NMR (*30*), and this allows a thorough comparison between the two oxidation states in solution. It should be noted that the existence of forms A and B causes static disorder in the X-ray electron density maps, thus preventing high resolution in this region (*69*); on the contrary, NMR provides data that allow individual characterization of the two forms.

The average minimized structures of the oxidized and reduced solution structures are shown in Figure 5. Overall, the RMSD values between them are 1.53 and 2.05 Å for backbone and heavy atoms, respectively. The RMSD per residue is reported in Figure 6 and is compared to the pairwise RMSD per residue within each family (reduced and oxidized), either superimposing the whole structures (A) or only three residues at a time (B). For large parts of the protein, the RMSD between the two average structures is larger than the RMSD within each family, indicating a significant difference. It is interesting to note that the region that superimposes best is that between 21 and 32, which contains the two antiparallel β strands constituting the central part of the β sheet. The helices forming the heme-binding pocket and the initial and terminal ones, in contrast, show relatively large RMSD values with higher values in regions 34−50, 54−64, and 73−75. However, the local conformations are well maintained as witnessed by the much lower RMSD values if the structures are compared only locally. Some conformational differences still remain at positions 40−42, 49, 60−64, and 74. This observation indicates that such differences may arise mainly from small changes in dihedral angles which propagate along the structure and induce relative movements of elements of secondary structures. To support this, Table 4 reports the RMSD values obtained by superimposing one element of secondary structure at a time. All these values are well below the global RMSD value of 1.53 Å for backbone atoms, indicating that locally the various elements of secondary structure are not so different. This suggests that the antiparallel β sheet 21−

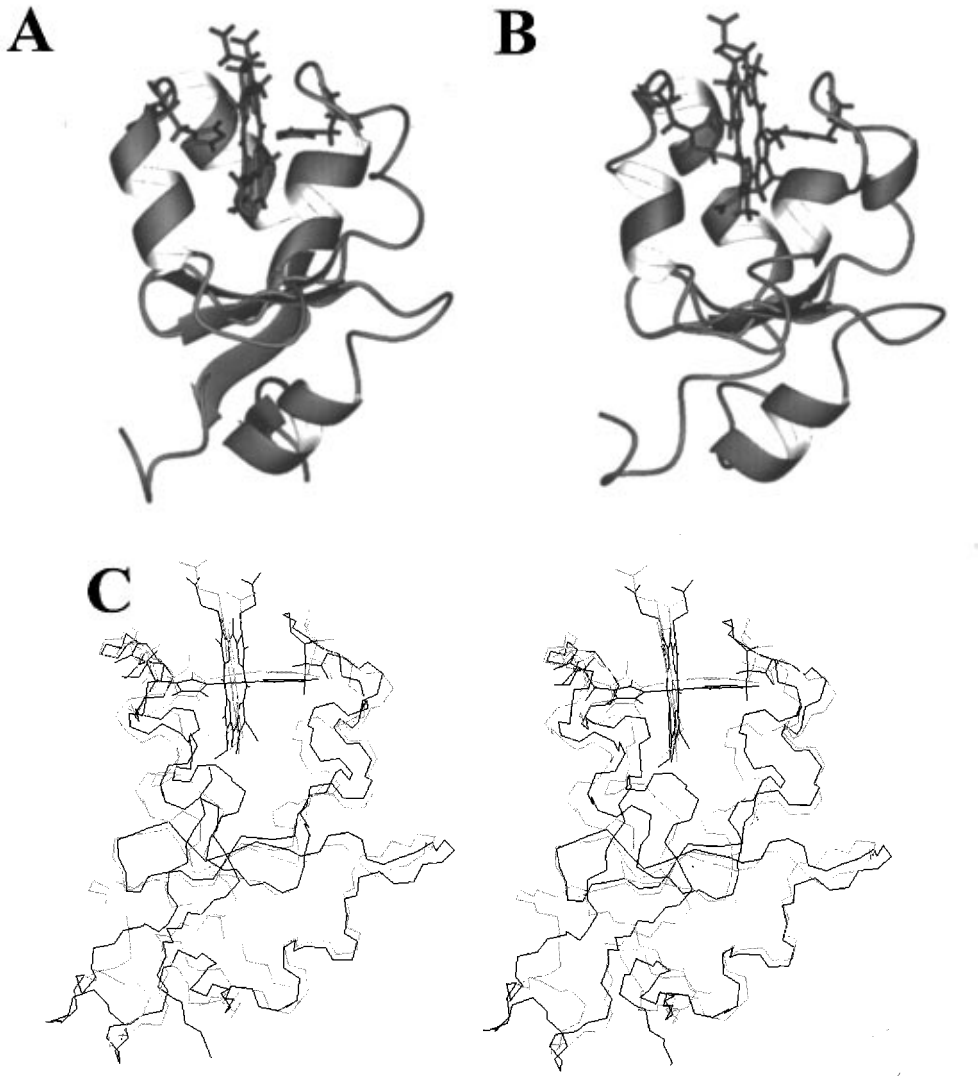


FIGURE 5: Ribbon diagram of the reduced (A) and oxidized (B) average minimized structures of rat microsomal cyt $b_5$. Also a stereoview of the two structures (oxidized, black; reduced, gray) is shown (C).

25/28−31 could function as a support around which the helices have the possibility to rearrange upon addition or removal of one electron. It is worth noting that the nonexchanging NH protons were mainly identified in this region. In particular, helices α2 and α4 are shifted on opposite sides with respect to the iron atom, shifted perpendicularly to the helix axis, toward the exterior of the protein. The other two helices forming the heme-binding pocket also show small translational movements. Interestingly, two of the acidic residues claimed to be involved in protein−protein recognition with cytochrome *c* (cyt *c* hereafter), namely, Asp 60 and Glu 56 (*75*−*77*), follow this redox state dependent conformational change, with a difference in the conformation of the carboxylate groups in the two forms of 3−4 Å. The rest of the acidic residues, which were suggested to interact with cyt *c*, are located on helix α3 which shows a slight translational movement parallel to the helix axis. The volume of the heme cavity, though, does not show globally significant variations. It is also very similar to that observed in the X-ray structure of the oxidized bovine isoenzyme. Only a conformational difference between the solution structures of the two oxidation states for residues 40−42 is observed which brings these surface-exposed residues closer to the heme in the oxidized state. This difference is documented by the absence of interresidue NOEs involving residues 40−42 in the reduced state, which instead were identified in the oxidized state.

The heme moiety is shifted toward the interior of the heme pocket in the oxidized with respect to the reduced state with differences in the average positions, greater than the spread within each family, on the side of methyls 1 and 8 and of propionate 7. The position of the heme in the X-ray structure of the oxidized bovine isoenzyme is intermediate between the two, slightly more similar to the oxidized form than to the reduced one. Propionate groups have claimed to play a role in the structure−function relationship and in molecular recognition in cyt $b_5$ (*69*, *78*, *79*) and in other cytochromes (*13*, *37*, *80*). Indeed, in the three cytochromes for which the solution structures have been determined in both oxidation states, a rearrangement of propionate 7 upon change of oxidation state has been invariantly observed (*13*, *37*, *80*). For cyt $b_5$, it has been suggested that propionate 7 has the function of stabilizing the extra positive charge in the oxidized state (*21*), while propionate 6, which is pointing toward the solution, is involved in molecular recognition (*69*, *78*, *79*). In the present oxidized rat cyt $b_5$, propionate 7 is

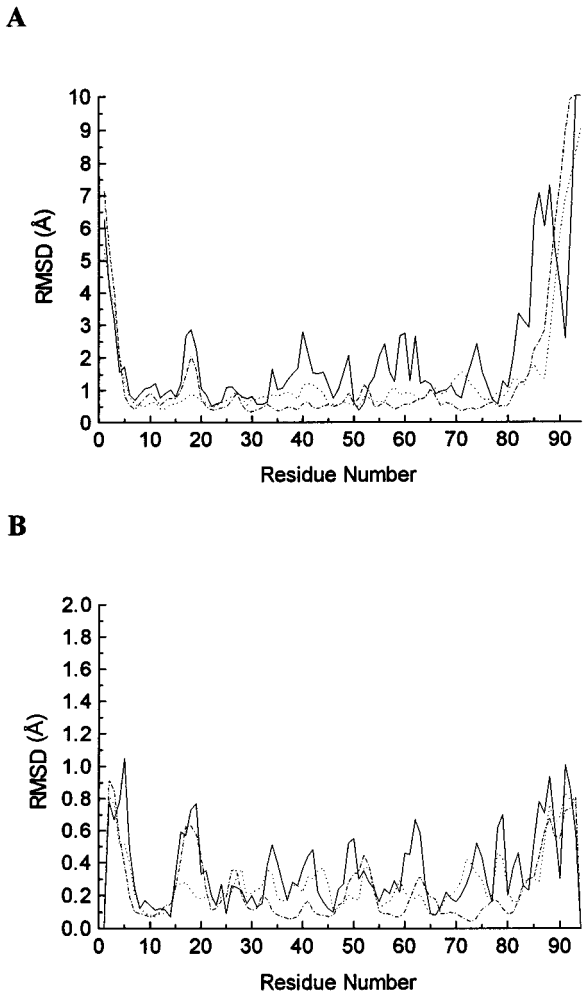


FIGURE 6: RMSD per residue for backbone atoms within the oxidized (long dashed line) and the reduced (short dashed line) families of structures, and between the average structures of the two families (solid line) superimposing either the whole structures (A) or only three residues at a time (B).

Table 4: Average RMSD Values for Backbone Atoms between the Oxidized and Reduced Average Minimized Structures of Rat Cyt $b_5$ Obtained Superimposing Only Residues Constituting a Defined Element of Secondary Structure at a Time

| residue range (secondary structure elements) | RMSD for backbone atoms (Å) |
|---|---|
| 21−25($\beta$4) and 28−32($\beta$3) | 0.30 |
| 33−39(α2) | 0.54 |
| 42−50(α3) | 0.52 |
| 54−62(α4) | 1.09 |
| 64−74(α5) | 0.67 |
| 8−14(α1) | 0.25 |
| 81−87(α6) | 0.57 |
| 5−7($\beta$1) and 75−78($\beta$2) | 0.59 |

well-defined and gives NOEs between its α protons and Pro 40 on one side of the heme ring and between its $\beta$ protons and Ser 64 on the other side. Its carboxylate group points toward the exterior of the heme but forms a hydrogen bond with the OH group of Ser 64. In the crystal structure of the oxidized bovine protein (*67*), the propionate conformation is similar, even if the carboxylate group is pointing toward the interior of the heme and forms a hydrogen bond with the NH of Ser 64. Propionate 6 displays a slightly smaller number of NOEs, thus becoming more disordered on the C$\beta$ and on the carboxylate. In the reduced state, propionates are less defined as a smaller number of NOEs were observed. However, a careful analysis showed that the NOEs between propionate 7 and residues 40 and 64, which should appear in a "clean" region of the 2D NOESY maps, are missing, outside the experimental error, while one NOE between an α proton and residue 61 is observed. This may indicate that propionate 7 has different conformations in the two oxidation states. Propionate 6, despite the lower definition, experiences minor structural differences.

Summarizing, the conformation of the reduced form seems to have a slightly wider surface on the side of the protein that is proposed to interact with cyt *c*, due to a displacement of helix α4, and the heme seems to be a little more exposed to the solvent, compared to the oxidized form. In parallel, propionate 7 gets closer to Ser 64, on passing from the reduced to the oxidized state.

*Amide Hydrogen Exchange*. The exchange rate of amide protons with the solvent changes drastically upon removal of one electron, as already observed for cyt *c* (*37*). In particular, while in the reduced state 39 backbone NHs were identified as nonexchangeable, this number drops to 16 in the oxidized state. This comparison was made by analyzing NOESY spectra acquired roughly 5 days after the protein, in each of the two states, was exchanged with $D_2O$ and is reported in Figure 1, where the filled and the open squares represent nonexchangeable NH protons for the oxidized and reduced proteins, respectively. The majority of NH groups which do not exchange in both oxidation states under the above conditions are located in $\beta$ strands $\beta$4, $\beta$2, and $\beta$3. For $\beta$ strands 2 and 3, several sequential NH protons are nonexchangeable. This is consistent with these two strands being quite buried in the protein frame. This is the region that better superimposes in both oxidation states and is proposed to play a structural support role for the heme pocket.

The NH groups that become nonexchangeable upon addition of one electron are located mainly in the helices forming the heme-binding pocket, in particular in helices α3 and α4, and in strand $\beta$1. The location of these residues in the protein frame is shown in Figure 7. Interestingly, a large part of these residues coincides with the most mobile parts observed in a 2.5 ns molecular dynamics simulation of cyt $b_5$ (*81*). The exchange with the solvent should occur through fluctuations that allow solvent molecules to interact with buried residues and thus to exchange (*35*, *36*, *82*, *83*). The two solution structures, which are time-averaged structures, are not so different as to justify an increased solvent accessibility of the oxidized state, and therefore it is possible that the increased NH exchange rates in the above mentioned parts are due to a greater flexibility in the oxidized state rather than in the reduced one. Figure 7 shows that the residues that have a different exchange rate depending on the oxidation state are mainly located on the side of the protein which contains most of the acidic residues (43, 44, 48, 56, 60) that should interact with cyt *c*, namely, in helix α4 and in part of helix α3. Also, scattered residues in the protein showing the same behavior exist, but in smaller number. The possibly larger mobility of the oxidized protein is also consistent with its lower thermal stability with respect to the reduced form (*84*).

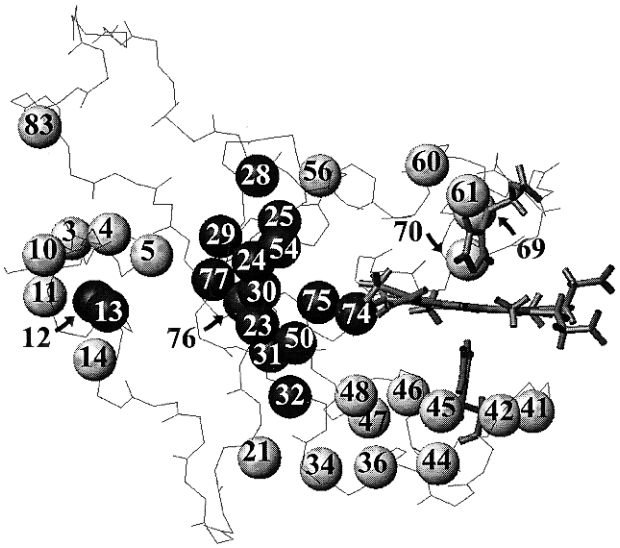


FIGURE 7: Mapping in the protein frame of NH protons experiencing different exchange properties in the two redox states. Nonexchangeable amide groups in both oxidation states are shown in black; those showing a different behavior in the two forms (nonexchangeable in the reduced state, exchangeable in the oxidized state) are shown in light gray. Besides these, only the heme and backbone atoms are shown.

For horse heart cytochrome *c*, for which there are a large number of studies aimed at understanding the forces driving complex formation with cyt $b_5$ (*75, 76, 85, 86*), the data for the oxidized protein are available (*13*), while they are not reported for the reduced form (*87*), which prevents a meaningful comparison. In the case of *S. cerevisiae* iso-1-cytochrome *c* instead, different NH exchange rates were observed for the two oxidation states (*14, 37*); the residues showing different behavior are mainly located around propionate 6, and involve five lysine residues, hinting at a possible region of interaction with cyt $b_5$.

*Comparison with Other Cyt $b_5$ Structures.* Several crystal structures of cyt $b_5$ from different sources are available. The bovine microsomal isoenzyme is easier to tackle due to the more favorable distribution between forms A and B (9:1), and a crystal structure of the oxidized form is available (*67*) (PDB entry 3b5c.pdb), which has been recently refined to 1.5 Å resolution (*68*) (PDB entry 1cyo.pdb). Also, a solution structure has recently become available for the bovine isoenzyme (*70*) (PDB entry 1wdb.pdb). Finally, rat cyt $b_5$ from the outer mitochondrial membrane was expressed (*88*) and the X-ray structure recently solved (*69*) (PDB entry 1b5m.pdb).

The solution structures of the rat (present paper) and bovine (*70*) oxidized proteins, which have a 94% homology, are significantly different, the pairwise RMSD between the two being 4.26 Å for backbone atoms. The solution structure of the bovine isoenzyme is characterized by a smaller number of NOE constraints with respect to the present one (1130 vs 1810), leading to a poorer resolution (RMSD 0.73 vs 0.50 Å for backbone atoms). This difference in the number of NOE constraints is most dramatic in the region of the protein around His 39, since no connectivities were identified for residue 34 and for residues 39−41 in the bovine isoenzyme, even though that study also relied on a $^{15}$N-labeled sample. This yields a structure characterized by no experimental constraints in that region, except those deriving from the known heme coordination. Therefore, some differences cannot be considered as real differences but the result of a poor resolution. On the other hand, the various elements of secondary structure, far from the paramagnetic center, are well-refined and relatively similar to the rat microsomal protein.

The solution structure of the bovine isoenzyme (*70*) is also different from its X-ray structure (*68*); the average RMSD for backbone atoms is 4.54 Å. Again residues in the proximity of the paramagnetic center have quite different conformations. The X-ray structure of rat microsomal cyt $b_5$ is not available; however, the present solution structure of rat cyt $b_5$ gives much closer results to the X-ray structure of the bovine isoenzyme.

*Comparison with the Apo Form.* The solution structures of rat cyt $b_5$ in both oxidation states can be compared with the recently obtained solution structure of the apoprotein (*89*). The average backbone pairwise RMSD values between the apo form and the oxidized and reduced average minimized structures are 4.32 and 4.21 Å, respectively, indicating that, even if the structure of the apoprotein is still quite well-defined in solution, this is rather different from the holo structure, of both oxidation forms. The differences are larger for the four helices forming the heme-binding pocket, in particular for the two on the sides of His 63, while they are smaller for the rest of the protein. The part that better superimposes, as already observed comparing the two oxidation states, is the $\beta$ strand involving residues 21−25 and 28−32. This again suggests that the role played by these strands is as a structural support for the heme-binding pocket.

## CONCLUSIONS

We have reported a high-quality structure of oxidized rat microsomal cyt $b_5$. Pseudocontact shifts were employed for the structure calculation and, while contributing very little to target function (indicating very good agreement with experimental data), they do contribute to increase the resolution, mainly in the areas near the paramagnetic center, where structural information is most important. Pseudocontact shifts are a "centered" type of constraint, centered on the metal ion, and thus contribute to define the heme pocket, in a radius of roughly 10 Å.

This has allowed the observation of structural differences between the oxidized and the reduced forms. Finally, comparison of the solution structures of the protein in the two oxidation states, combined with the dynamic information obtained from NH exchange rates, gives precious insights into understanding the electron transfer mechanism. The differential behavior of NH exchange rates for cyt $b_5$ upon loss of one electron was found located primarily in the region of the protein that should interact with cyt *c*, even if also scattered residues show the same behavior. Also for cyt *c* the number of nonexchanging protons in comparable conditions is much larger for the reduced protein, hinting at a lower mobility with respect to the oxidized state. In complex formation between cyt *c* and cyt $b_5$, the potentials are such that reduced cyt $b_5$ should "pass" its electron to cyt *c*. It seems so far a general trend that reduced forms are less flexible than the oxidized ones. It would be tempting to speculate that, in order to optimize electron transfer, the reduced protein could provide a less flexible structure with

a suitable conformation for the interaction with a redox partner (slightly more open heme cleft on the side of acidic residues, and with the heme a little more exposed), while the oxidized partner would be more flexible, providing an adaptable module able to easily assume several conformations around the average structure to achieve complex formation. After the electron has been transferred, the situation between the two redox partners should be inverted. For example, in the case of the cyt $b_5$−cyt *c* complex, after electron transfer, cyt $b_5$ would become more flexible and with a slightly different conformation, while cyt *c* would become less flexible and ready to reduce another protein. This would be coupled to the change in conformation of propionate 7. It should be noted that the conformational differences we are observing are small displacement of groups (propionate 7) or small variations of dihedral angles that cause detectable displacements by propagating along pieces of secondary structural elements. However, the small structural variations are in agreement with expectations based on electron transfer theory; that is, no large structural rearrangements should be coupled to electron transfer in biological macromolecules.

## ACKNOWLEDGMENT

We thank Prof. S. G. Sligar for generously providing the gene encoding the soluble fragment of rat microsomal cyt $b_5$ and Filippo Ferroni for preparing the protein sample.

## SUPPORTING INFORMATION AVAILABLE

The $^1$H chemical shifts, the experimental NOE intensities used for the structure calculations, and the list of stereospecific assignments are available (21 pages). Ordering information is given on any current masthead page.

## REFERENCES

1. Wüthrich, K. (1986) in *NMR of Proteins and Nucleic Acids*, Wiley, New York.
2. Clore, G. M., and Gronenborn, A. M. (1991) *Science 252*, 1390−1399.
3. Clore, G. M., and Gronenborn, A. M. (1994) *Protein Sci. 3*, 372−390.
4. Schmitz, U., and James, T. L. (1992) *J. Am. Chem. Soc. 114*, 10654−10656.
5. Torda, A. E., Scheek, R. M., and van Gunsteren, W. F. (1990) *J. Mol. Biol. 214*, 223−235.
6. Torchia, D. A. (1996) in *Encyclopedia of Nuclear Magnetic Resonance* (Grant, D. M., and Harris, R. K., Eds.) pp 3785−3790, John Wiley and Sons, Chichester, U.K.
7. Wagner, G. (1993) *Curr. Opin. Struct. Biol. 3*, 748−754.
8. Guss, J. M., Harrowell, P. R., Murata, M., Norris, V. A., and Freeman, H. C. (1986) *J. Mol. Biol. 192*, 361−387.
9. Scott, R. A., and Mauk, A. G. (1996) in *Cytochrome c. A multidisciplinary approach*, University Science Books, Sausalito, CA.
10. Banci, L., Bertini, I., Eltis, L. D., Felli, I. C., Kastrau, D. H. W., Luchinat, C., Piccioli, M., Pierattelli, R., and Smith, M. (1994) *Eur. J. Biochem. 225*, 715−725.
11. Bertini, I., Luchinat, C., and Rosato, A. (1996) *Prog. Biophys. Mol. Biol. 66*, 43−80.
12. Banci, L., Bertini, I., De la Rosa, M. A., Koulougliotis, D., Navarro, J. A., and Walter, O. (submitted for publication).
13. Banci, L., Bertini, I., Gray, H. B., Luchinat, C., Reddig, T., Rosato, A., and Turano, P. (1997) *Biochemistry 36*, 9867−9877.
14. Baistrocchi, P., Banci, L., Bertini, I., Turano, P., Bren, K. L., and Gray, H. B. (1996) *Biochemistry 35*, 13788−13796.
15. Banci, L., Bertini, I., Quacquarini, G., Walter, O., Diaz, A., Hervás, M., and De la Rosa, M. A. (1996) *JBIC 1*, 330−340.
16. Banci, L., Bertini, I., Dikiy, A., Kastrau, D. H. W., Luchinat, C., and Sompornpisut, P. (1995) *Biochemistry 34*, 206−219.
17. Bertini, I., Eltis, L. D., Felli, I. C., Kastrau, D. H. W., Luchinat, C., and Piccioli, M. (1995) *Chemistry—A European Journal 1*, 598−607.
18. Bertini, I., Dikiy, A., Kastrau, D. H. W., Luchinat, C., and Sompornpisut, P. (1995) *Biochemistry 34*, 9851−9858.
19. Pettigrew, G. W., and Moore, G. R. (1987) in *Cytochromes c; Biological Aspects*, Springer-Verlag, Berlin.
20. von Bodman, S. B., Schulder, M. A., Jollie, D. R., and Sligar, S. G. (1986) *Proc. Natl. Acad. Sci. U.S.A. 83*, 9443−9447.
21. Mathews, F. S. (1985) *Prog. Biophys. Mol. Biol. 45*, 1−56.
22. Ito, A., and Sato, R. (1968) *J. Biol. Chem. 243*, 4922−4923.
23. Spatz, L., and Strittmatter, P. (1971) *Proc. Natl. Acad. Sci. U.S.A. 68*, 1042−1046.
24. Oshino, N., Imai, Y., and Sato, R. (1971) *J. Biochem. (Tokyo) 69*, 155−167.
25. Strittmatter, P., Spatz, L., Corcoran, D., Rogers, M. J., Setlow, B., and Redline, R. (1974) *Proc. Natl. Acad. Sci. U.S.A. 71*, 4565−4569.
26. Hildebrandt, A., and Estabrook, R. W. (1971) *Arch. Biochem. Biophys. 143*, 66−79.
27. Imai, Y., and Sato, R. (1977) *Biochem. Biophys. Res. Commun. 75*, 420−426.
28. Hegesh, E., Hegesh, J., and Kaftory, A. (1986) *N. Engl. J. Med. 314*, 757−761.
29. Strittmatter, P., and Ozols, J. (1966) *J. Biol. Chem. 241*, 4787−4792.
30. Banci, L., Bertini, I., Ferroni, F., and Rosato, A. (1997) *Eur. J. Biochem. 249*, 270−279.
31. Marcus, R. A., and Sutin, N. (1985) *Biochim. Biophys. Acta 811*, 265−275.
32. Bertini, I., Gray, H. B., Lippard, S. J., and Valentine, J. S. (1994) in *Bioinorganic Chemistry*, University Science Books, Mill Valley, CA.
33. Barbato, G., Ikura, M., Kay, L. E., Pastor, R. W., and Bax, A. (1992) *Biochemistry 31*, 5269−5278.
34. Ernst, R. R. (1994) *Pure Appl. Chem. 66*, 1955−1960.
35. Bai, Y. W., Sosnick, T. R., Mayne, L., and Englander, S. W. (1995) *Science 269*, 192−197.
36. Englander, S. W. (1992) *Science 256*, 1684.
37. Banci, L., Bertini, I., Bren, K. L., Gray, H. B., Sompornpisut, P., and Turano, P. (1997) *Biochemistry 36*, 8992−9001.
38. Macura, S., Wüthrich, K., and Ernst, R. R. (1982) *J. Magn. Reson. 47*, 351−357.
39. Marion, D., and Wüthrich, K. (1983) *Biochem. Biophys. Res. Commun. 113*, 967−974.
40. Banci, L., Bertini, I., Luchinat, C., Piccioli, M., Scozzafava, A., and Turano, P. (1989) *Inorg. Chem. 28*, 4650−4656.
41. Bax, A., and Davis, D. G. (1985) *J. Magn. Reson. 63*, 207−213.
42. Griesinger, C., Otting, G., Wüthrich, K., and Ernst, R. R. (1988) *J. Am. Chem. Soc. 110*, 7870−7872.
43. Piotto, M., Saudek, V., and Sklenar, V. (1992) *J. Biomol. NMR 2*, 661−666.
44. Eccles, C., Güntert, P., Billeter, M., and Wüthrich, K. (1991) *J. Biomol. NMR 1*, 111−130.
45. Güntert, P., Braun, W., and Wüthrich, K. (1991) *J. Mol. Biol. 217*, 517−530.
46. Mc Connell, H. M. (1972) *Proc. Natl. Acad. Sci. U.S.A. 69*, 335.
47. Mc Connell, H. M., and McGarvey, B. R. (1973) in *NMR of Paramagnetic Molecules*, Academic Press, New York.
48. Bertini, I., and Luchinat, C. (1986) in *NMR of paramagnetic molecules in biological systems*, Benjamin/Cummings, Menlo Park, CA.
49. Bertini, I., and Turano, P. (1994) in *NMR of paramagnetic macromolecules, NATO ASI Series* (La Mar, G. N., Ed.) Kluwer Academic, Dordrecht.
50. Bertini, I., and Luchinat, C. (1996) in *NMR of paramagnetic substances, Coord. Chem. Rev. 150*, Elsevier, Amsterdam.

51. Güntert, P., Mumenthaler, C., and Wüthrich, K. (1997) *J. Mol. Biol. 273*, 283−298.
52. Banci, L., Bertini, I., Bren, K. L., Cremonini, M. A., Gray, H. B., Luchinat, C., and Turano, P. (1996) *JBIC 1*, 117−126.
53. Banci, L., Bertini, I., Gori Savellini, G., Romagnoli, A., Turano, P., Cremonini, M. A., Luchinat, C., and Gray, H. B. (1997) *Proteins: Struct., Funct., Genet. 29*, 68−76.
54. Pearlman, D. A., and Case, D. A. (1991) in *SANDER*: University of California, San Francisco, CA.
55. Laskowski, R. A., MacArthur, M. W., Moss, D. S., and Thornton, J. M. (1993) *J. Appl. Crystallogr. 26*, 283−291.
56. Laskowski, R. A., Rullmann, J. A. C., MacArthur, M. W., Kaptein, R., and Thornton, J. M. (1996) *J. Biomol. NMR 8*, 477−486.
57. Borgias, B., Thomas, P. D., and James, T. L. (1989) in *Complete Relaxation Matrix Analysis (CORMA)*, University of California, San Francisco, CA.
58. Veitch, N. C., Whitford, D., and Williams, R. J. P. (1990) *FEBS Lett. 269*, 297−304.
59. Guiles, R. D., Basus, V. J., Sarma, S., Malpure, S., Fox, K. M., Kuntz, I. D., and Waskell, L. (1993) *Biochemistry 32*, 8329−8340.
60. Guiles, R. D., Basus, V. J., Kuntz, I. D., and Waskell, L. (1992) *Biochemistry 31*, 11365−11375.
61. Sarma, S., DiGate, R. J., Banville, D., and Guiles, R. D. (1996) *J. Biomol. NMR 8*, 171−183.
62. Lee, K.-B., La Mar, G. N., Mansfield, K. E., Smith, K. M., Pochapsky, T. C., and Sligar, S. G. (1993) *Biochim. Biophys. Acta 1202*, 189−199.
63. Banci, L., Bertini, I., Pierattelli, R., and Vila, A. J. (1994) *Inorg. Chem. 33*, 4338−4343.
64. Banci, L., Pierattelli, R., and Turner, D. L. (1995) *Eur. J. Biochem. 232*, 522−527.
65. Keller, R. M., and Wüthrich, K. (1980) *Biochim. Biophys. Acta 621*, 204−217.
66. McLachlan, S. J., La Mar, G. N., Burns, P. D., Smith, K. D., and Langry, K. C. (1986) *Biochim. Biophys. Acta 874*, 274−284.
67. Mathews, F. S., Argos, P., and Levine, M. (1972) *Cold Spring Harbor Symp. Quant. Biol. 36*, 387.
68. Durley, R. C. E., and Mathews, F. S. (1996) *Acta Crystallogr. D52*, 65−72.
69. Rodriguez Maranon, M. J., Qiu, F., Stark, R. E., White, S. P., Zhang, X., Foundling, S. I., Rodriguez, V., Schilling, C. L., Bunce, R. A., and Rivera, M. (1996) *Biochemistry 35*, 16378−16390.
70. Muskett, F. W., Kelly, G. P., and Whitford, D. (1996) *J. Mol. Biol. 258*, 172−189.
71. Argos, P., and Mathews, F. S. (1975) *J. Biol. Chem. 250*, 747−751.
72. Kabsh, W., and Sander, C. (1983) *Biopolymers 22*, 2577−2637.
73. Oosterhuis, W. T., and Lang, G. (1969) *Phys. Rev. 178*, 439−456.
74. Emerson, S. D., and La Mar, G. N. (1990) *Biochemistry 29*, 1556−1566.
75. Salemme, F. R. (1976) *J. Mol. Biol. 102*, 563−568.
76. Rodgers, K. K., Pochapsky, T. C., and Sligar, S. G. (1988) *Science 240*, 1657−1659.
77. Northrup, S. H., Thomasson, K. A., Miller, C. M., Barker, P. D., Eltis, L. D., Guillemette, J. G., Inglis, S. C., and Mauk, A. G. (1993) *Biochemistry 32*, 6613−6623.
78. McLachlan, S. J., La Mar, G. N., and Sletten, E. (1986) *J. Am. Chem. Soc. 108*, 1285−1291.
79. Mathews, F. S. (1980) *Biochim. Biophys. Acta 622*, 375−379.
80. Ferrer, J. C., Turano, P., Banci, L., Bertini, I., Morris, I. K., Smith, K. M., Smith, M., and Mauk, A. G. (1994) *Biochemistry 33*, 7819−7829.
81. Storch, E. M., and Daggett, V. (1995) *Biochemistry 34*, 9682−9693.
82. Hvidt, A., and Nielsen, S. O. (1966) *Adv. Protein Chem. 21*, 287.
83. Englander, S. W., and Kallenbach, N. R. (1983) *Q. Rev. Biophys. 16*, 521−655.
84. Kitagawa, T., Sugiyama, T., and Yamano, T. (1982) *Biochemistry 21*, 1680−1686.
85. Wendoloski, J. J., Matthew, J. B., Weber, P. C., and Salemme, F. R. (1987) *Science 238*, 794−797.
86. Guiles, R. D., Sarma, S., DiGate, R. J., Banville, D., Basus, V. J., Kuntz, I. D., and Waskell, L. (1996) *Nat. Struct. Biol. 3*, 333−339.
87. Qi, P. X., Di Stefano, D. L., and Wand, A. J. (1994) *Biochemistry 33*, 6408−6417.
88. Rivera, M., Barillas-Mury, C., Christensen, K. A., Little, J. W., Wells, M. A., and Walker, F. A. (1992) *Biochemistry 31*, 12233−12240.
89. Falzone, C. J., Mayer, M. R., Whiteman, E. L., Moore, C. D., and Lecomte, J. T. J. (1996) *Biochemistry 35*, 6519−6526.
90. Koradi, R., Billeter, M., and Wüthrich, K. (1996) *J. Mol. Graphics 14*, 51−55.

BI971896W